Li et al. Nanoscale Research Letters (2016) 11:441
DOI 10.1186/s11671-016-1651-y

Nanoscale Research Letters

NANO EXPRESS Open Access

Fabrication of $NaYF_4$:Yb,Er Nanoprobes for Cell Imaging Directly by Using the Method of Hydrion Rivalry Aided by Ultrasonic

Zhihua Li*, Haixia Miao, Ying Fu, Yuxiang Liu, Ran Zhang and Bo Tang*

Abstract

A novel method of fabricating water-soluble bio-probes with ultra-small size such as $NaYF_4$:Yb,Er (18 nm), $NaGdF_4$:Yb,Er (8 nm), CaF_2:Yb,Er (10 nm), PbS (7 nm), and ZnS (12 nm) has been developed to provide for the solubility switch of nanoparticles from oil-soluble to water-soluble in terms of hydrion rivalry aided by ultrasonic. Using $NaYF_4$:Yb,Er (18 nm) as an example, we evaluate the properties of as-prepared water-soluble nanoparticles (NPs) by using thermogravimetric analyses (TGA), Fourier transform infrared spectroscopy (FTIR), zeta potential (ζ) testing, and 1H nuclear magnetic resonance (^{1}HNMR). The measured ζ value shows that the newly prepared hydrophilic $NaYF_4$:Yb,Er NPs are the positively charged particles. Acting as reactive electrophilic moiety, the freshly prepared hydrophilic $NaYF_4$:Yb,Er NPs have carried out the coupling with amino acids and fluorescence labeling and imaging of HeLa cells directly. Experiments indicate that the method of hydrion rivalry aided by ultrasonic provides a simple and novel opportunity to transform hydrophobic NPs into hydrophilic NPs with good reactivity, which can be imaging some specific biological targets directly.

Keywords: Hydrion rivalry aided by ultrasonic, $NaYF_4$:Yb,Er, Bioimaging, Nanoprobe

Background

In recent years, fluorescent label materials focus on the up-conversion (UC) phosphors represented by $NaYF_4$:Yb,Er owing to their unique properties of emission light at shorter wavelengths (visible and near-infrared) after excitation in the near-infrared. Compared with conventional fluorescent materials, such as rhodamine, fluorescein, isothiocyanates, cyanine dyes [1, 2], and quantum dots [3–7], the luminous feature of up-conversion nanoparticles (UCNPs) dramatically reduces background autofluorescence since endogenous fluorophores are not excited by the longer excitation wavelengths, which results in high target-to-background ratios [8, 9], minimizing photodamage [10] and good tissue penetration [8, 9, 11–13]. UCNPs have become a kind of highly promising fluorescence labeling materials for biological applications.

Acting as bio-probes, the prepared UCNPs should meet some requirements of high fluorescent intensity [9, 14], small diameter [15], water-soluble [16, 17], low cytotoxicity [15, 18–21], etc. So, the control synthesis of UCNPs becomes to be crucial and attracts considerable interest in recent years [22–29]. To date, employing oleic acid (OA, $C_{17}H_{33}COOH$) to act as reaction media to obtain UCNPs with controlled size and morphology has been still a popular synthesis route [30–33]. Despite going well, the inherent shortcomings of OA layer covered on the as-prepared UCNP surface may prevent widespread use of UCNPs in practical biological settings. It is known that the OA layer covered on the surface of as-prepared UCNPs not only decreases the fluorescence intensity of UCNPs [16, 18] but also hinders their bio-application directly because of the water-soluble environment of biological fluids, namely, it is the necessary prerequisite to modify the surface of these NPs before applying into biomedical science. The advantages of surface functionalization of these NPs are not only to render them reasonably water-soluble and biocompatible but also to provide active sites for subsequent coupling with biological or chemical

* Correspondence: lizhihua2006@126.com; tangbo@sdnu.edu.cn
Key Laboratory of Molecular and Nano Probes, College of Chemistry, Chemical Engineering and Materials Science, Collaborative Innovation Center of Functionalized Probe for Chemical Imaging in Universities of Shandong, Shandong Normal University, Jinan 250014, China

moieties [34–41]. So far, many attempts have been made to transform the oil-soluble OA-capped UCNPs into water-soluble, such as polymer capping [42, 43], surface silanization [44], OA-capped $NaYF_4$:Yb,Er NP coating by hydrophilic group [45, 46], ligand exchange [47], ligand oxidation [48–50], hydrochloric acid [16], and layer-by-layer method [51]. Unfortunately, all of the post-treatments are time-consuming and may lead to aggregation; furthermore, the surface modified UCNPs always have bigger size than that of before.

Recently, we have studied the relationships between coating layer (OA) and $NaYF_4$:Yb,Er in detail and come up with an easily operated physical method, ultrasonic separation, to remove the oleate ligand from the surface of OA-capped $NaYF_4$:Yb,Er NPs [52]. Unfortunately, the ultrasonic separation method is hardly applied to the particles whose sizes are smaller than 20 nm, because a smaller $NaYF_4$ particle will have a greater surface-to-volume ratio than the bigger one, and therefore displays a much greater surface free energy, which induces the growth and aggregation under the function of ultra-sound treatment. For application in vivo imaging, the size of UCNPs should be less than 10 nm [15]. In general, particles with dimension of 6 nm in diameter are the renal excretion limit size [53], and these ultra-small particles are excreted via the kidney and mostly excreted through the liver and into the bile without significant metabolism [54]. Even if UCNPs can be made especially small, these particles may become very bigger after water-soluble modification by currently common method, and the size of particles cannot meet the requirements for acting as nanobiotag to apply to the intracellular tracking of biomolecules. Recognizing the importance of water-soluble post-treatment of OA-capped UCNPs and how to develop a facial way to achieve for the solubility switch of NPs from oil-soluble to water-soluble meanwhile keeping the size and optical properties unchanged after treatment is challenging.

As known to all, the surface of $NaYF_4$:Yb,Er NPs synthesized in OA reaction medium exists a fair amount of electron-poor metal atoms Y, which can coordinate with the carboxy groups of oleate anions. Considering OA is a weak acid, H^+ will bond with oleate anions ($C_{17}H_{33}COO^-$) easily if H^+ is added into the above solution. Or rather, the positively charged $NaYF_4$:Yb,Er NPs coming from electron-poor metal atoms Y and H^+ have competitive reaction with $C_{17}H_{33}COO^-$ in the solution. Considering "ultrasonic separation" also works well, it is expected that removing the oleate ligand from the surface of OA-capped NPs will be much easier by using of hydrion rivalry aided by ultrasonic.

Herein, we present a universal protocol, hydrion rivalry aided by ultrasonic, to remove the oleate ligand from the surface of OA-capped NPs. OA-capped ultra-small NPs, including $NaYF_4$:Yb,Er (18 nm), $NaGdF_4$:Yb,Er (8 nm), CaF_2:Yb,Er (10 nm), PbS (7 nm), and ZnS (12 nm), act as examples to illustrate the transformation from oil-soluble NPs to water-soluble NPs. Considering after the removing of negatively charged oleate from the surface of $NaYF_4$:Yb,Er, the newly prepared OA-free $NaYF_4$:Yb,Er NPs may carry some positive charges, which will turn into reactive electrophilic moiety. We test the zeta potential of the freshly prepared water-soluble $NaYF_4$:Yb,Er NPs and demonstrate the newly prepared OA-free $NaYF_4$:Yb,Er NPs how to couple with amino acids and mark HeLa cells directly.

Methods

Materials

All of the commercially available reagents are purchased and unpurified. Rare-earth oxide (Y_2O_3, Yb_2O_3, Er_2O_3, Gd_2O_3, 99.9 %, Sigma), dichloride ($CaCl_2$, $PbCl_2$, $ZnCl_2$, 99.9 %, Sigma), Na_2S (99.9 %, Sigma), oleic acid (OA; 90 %, Sigma), 1-octadecene (ODE; >90 %, Sigma), absolute ethanol (>99.5 %, Sigma), cyclohexane (>90 %, Sigma), and rare-earth chlorides ($LnCl_3{\cdot}6H_2O$, Ln = Y, Yb, Er, Y:Yb:Er = 80:18:2 in molar ratio) are prepared by ourselves.

Synthesis of OA-Capped $NaYF_4$:Yb,Er NPs

At first, the molar ratio of Er_2O_3, Yb_2O_3, and Y_2O_3 is 2 %:18 %:80 %, which are mixed and dissolved in hydrochloric acid solution and heated to form a clear solution. The above solution is evaporated and crystallized to obtain rare-earth chlorides ($LnCl_3$). Second, 1 mmol dried $LnCl_3$ with 6 ml of OA and 14 ml of ODE are added into a three-necked flask. The mixture is stirred and heated under vacuum to 150 °C to form a homogeneous solution A and then cooled down to room temperature. Then, another mixed transparent solution B (0.1 g NaOH, 0.148 g NH_4F, and 10 ml of methanol) is added into solution A and then heated to 100 °C for 10 min. After methanol is evaporated thoroughly, the mixture is heated to 331 °C under nitrogen atmosphere for 60~90 min. Finally, the OA-capped $NaYF_4$:Yb,Er NPs are obtained after the precipitate is centrifuged and washed with ethanol/cyclohexane (v/v = 1:1) for three times, which can be easily redispersed in various nonpolar organic solvents (e.g., hexane, cyclohexane, toluene).

Synthesis of Oleate-Capped and OA-Free CaF_2:Yb,Er, PbS, ZnS, and $NaGdF_4$:Yb,Er Nanocrystals

The detailed experimental procedural is in the Additional file 1.

Fabrication of Ligand-Free NPs

The as-obtained OA-capped NPs (0.5 g) is added into 10 ml ethanol, then adjusting the pH value of the solution to 4.5 by using diluted hydrochloric acid (0.1 mol/l). Simultaneously, the mixture is stirred vigorous and

ultrasonic (power outlet 25–50 W) for 10~30 min, and then, the precipitate is separated by centrifugation. Finally, the hydrophilic NPs were washed with deionized water for two times and dried under vacuum at 60 °C.

UCNPs Coupling with Amino Acid

Fifty-milligram amino acid is added into 10-ml water, and the mixture is stirred to form a homogeneous and transparent solution. Then, 20 mg of new-UCNPs (18 nm) is added into the above solution and vigorously stirred for overnight at 25 °C. The complex of amino acid UCNPs is obtained by centrifugation.

Cell Culture, Fluorescent Labeling, and Imaging

The HeLa cells are cultured (at 37 °C, 5 % CO_2) on glass chamber slides in RPMI 640 medium containing 10 % fetal bovine serum and 1 % penicillin/streptomycin overnight in a culture box (Heraeus BB16UV). The cells are gently washed three times with PBS and blocked in PBS containing 1 % bovine serum albumin (BSA) for 20 min at 4 °C. Then, HeLa cells are incubated with new-UCNPs (18 nm, 10 μg/ml) at 4 °C for 0.5–24 h. Prior to imaging, the live cells are washed thoroughly with PBS to remove any unbound reagents. Cell imaging is performed on a Leica DMIL inverted fluorescence microscope (with a ×40/0.5 objective) equipped with a 980-nm NIR laser and a Nikon digital camera.

X-ray Diffraction

The samples are characterized by X-ray powder diffractometer (XRD) through using a Brucker D8-advance X-ray Diffractometer with Cu **K**α radiation (λ = 1.5418 Å); the operation voltage and current are, respectively, 40 kV and 40 mA. The 2θ range scan is swept from 10° to 70° in 0.02° steps with a count time of 0.2 s.

TEM

Particle sizes and shapes are characterized by an H-7650 (HITACHI, Japan) low- to high-resolution transmission electron microscope (HRTEM) operated at 100 kV. Samples are prepared by drying a drop of nanocrystal dispersion in cyclohexane/toluene (1/1) or ethanol on amorphous carbon-coated copper grids.

TGA

Thermogravimetric analyses are recorded on a TA Instrument SDT 2960 simultaneous DTA-thermogravimetric analyses (TGA) at a heating rate of 10 °C/min under N_2.

FTIR

The IR spectrum is obtained by using Brucker TENSOR Infrared Spectrometer.

NMR

The NMR measurement is carried out on Bruker BioSpin GmbH Spectrometer.

Zeta Potential

The zeta potential measurements are carried out on a Zeta PALS zeta potential analyzer (Brookhaven Instruments Corporation) at room temperature.

Confocal Fluorescence Imaging of Incubated Living Cells

UCNP-labeled HeLa cells are characterized by a modified Olympus FV1000 laser scanning confocal microscope equipped a continuous-wave (CW) NIR laser operating at 980 nm (Connet Fiber Optics, China). A ×60 oil-immersion objective lens is used to carry out the FL imaging of UCNP-labeled HeLa cells. The emission of active UCNPs is collected at 540 ± 20 and 660 ± 20 nm under the 980-nm CW laser excitation.

Results and Discussion

Mechanism of Removing Oleate Ligand from the Surface of $NaYF_4$:Yb,Er NPs

During the synthesis of NPs, OA acts as reaction media and takes part in the reaction. Before the reaction, OA reacts with Ln^{3+} ions to form $Ln(OA)_3$, which renders $LnCl_3$ disperses into the reaction system to ensure the homogeneous nucleation in the reaction. After the reaction, the carboxy group of oleate anions act as electron donors to coordinate with the rear earth ions possessing electron-poor and unsaturated bonding located at the surface of $NaYF_4$:Yb,Er, which leads to a layer of OA covered on the surface of as-prepared $NaYF_4$:Yb,Er. The bonding force between oleate and rear earth ions is weaker than that of normal chemical bond, which lies between physisorption and chemisorption, and can be separated by high-power ultrasonic wave [48]. However, the ultra-small particles, especially for the particles with their size less than 20 nm, have greater surface free energy, which always aggregate when using relatively high ultrasonic power to get rid of the OA layer from their surface. Therefore, how to eliminate the OA layer covered on the $NaYF_4$:Yb,Er NPs under low ultrasonic power is an intractable problem.

As stated above, the surface of the as-synthesized $NaYF_4$:Yb,Er NPs has a certain amount of positive charge, which can absorb the electronegative ions such as oleate to form OA-capped $NaYF_4$:Yb,Er NPs. If H^+ is introduced into the disperse system, the electrophilic substitution will occur that H^+ replaces the positively charged NPs of $NaYF_4$: Yb, Er to form a more stable weak acid, namely, oleic acid. Bogdan et al. carry out the transformation of oil-soluble to water-soluble $NaYF_4$:Yb,Er NPs by using this principle [16]. Unfortunately, their experiments are a time-consuming process with very low yield.

In our experiments, we adopt ultrasonic separation under weak acid to achieve the removing OA from OA-capped $NaYF_4$:Yb,Er NPs. The mechanism of removing oleate ligand from the surface of $NaYF_4$:Yb,Er NPs by using the way of hydrion rivalry aided by ultrasonic is showed in Fig. 1a. The H^+ ion will attack the conjunction of the carboxyl and the rear earth atom of $NaYF_4$:Yb,Er NPs, that is electrophilic substitution, namely, H^+ ions and Ln^{x+} of $NaYF_4$:Yb,Er NPs compete against each other to combine with carboxyl groups. What is more, H^+ ions' combination with oleate becomes much easy owing to the assistance of low-power ultrasonic; meanwhile, there is no agglomerative phenomenon for the ultrafine particles of $NaYF_4$:Yb,Er (less than 20 nm). The formation of weak electrolyte, $C_{17}H_{33}COOH$, also promotes the reaction process.

The Characterization of Samples

In our experiments, $NaYF_4$:Yb,Er (18 nm), $NaGdF_4$:Yb,Er (8 nm), CaF_2:Yb,Er (10 nm), PbS (7 nm), and ZnS (12 nm) have been synthesized to testify the removing OA effect by using the method of hydrion rivalry aided by ultrasonic (Additional file 1). Herein, the as-prepared $NaYF_4$:Yb,Er (18 nm) acts as a typical example to demonstrate our research.

The transmission electron microscopy (TEM) images, the digital pictures, and XRD spectra of as-prepared $NaYF_4$:Yb,Er NPs and OA-free $NaYF_4$:Yb,Er NPs are shown in Fig. 2. As can be seen, the OA-capped $NaYF_4$:Yb,Er NPs with the size of 18 nm are dispersed well in cyclohexane (1 mg/ml) (Fig. 2a). Figure 2b shows that the OA-capped $NaYF_4$:Yb,Er treated by using ultrasonic power (40 W) under weak acid (pH ≈ 4) for 15 min can easily disperse in ethanol (1 mg/ml). The size of particles is approximately 18 nm with polyhedron morphology, and their size and shape of the samples have almost unchanged after post-treatment (Fig. 2b). Figure 2c shows the digital pictures of three clear solutions (OA-capped $NaYF_4$:Yb,Er dispersed in cyclohexane, OA-free $NaYF_4$:Yb,Er dispersed in ethanol and deionized water, respectively) radiated by 980 nm laser, all of the solution concentration here is 1 mg/ml. Figure 2d depicts the XRD curve of the as-prepared $NaYF_4$:Yb,Er crystallizes with the β-phase of $NaYF_4$, all of the diffraction peaks are lined with the data of JCPDS No.16-0334. The calculated size of the as-prepared particles is 18.2 nm according to the Debye-Scherrer equation, which agrees with the result from the TEM study.

Figure 3a shows the TGA studies of the OA-capped $NaYF_4$:Yb,Er NPs and OA-free $NaYF_4$:Yb,Er NPs, respectively. Being synthesized in the assistance of OA surfactant, the surface of as-prepared $NaYF_4$:Yb,Er has been covered a layer of oleate, namely, OA-capped. Therefore, the measured curve of OA-capped $NaYF_4$:Yb,Er NPs shows two transformation points located at about 225 and 475 °C, respectively (Fig. 3a). The first weight loss stage is about 4.3 wt.% in the range of 30–250 °C which comes from the water loss. The second weight loss is 12.5 wt.% in the range of 250–600 °C, which is attributed to the combustion of the OA layer attached on the surface of sample. After samples are processed by using the method of hydrion rivalry aided by ultrasonic, the total weight loss is only about 2.2 wt.% and much lower than that of the untreated sample (4.3 + 12.5 %), which indicates that the weight loss of 2.2 wt.% is ascribed to the water loss, and the OA layer has been removed from the surface of as-prepared $NaYF_4$:Yb,Er NPs.

The measured FTIR absorption spectra of as-prepared $NaYF_4$:Yb,Er NPs before and after removing OA layer are showed in Fig. 3b. The FTIR spectrum of oleic acid is measured acting as the comparison experiment, which is depicted as curve a. For oleic acid, the specific absorbing peak of the alkene stretchings (C=C) and the asymmetric and symmetric stretching vibrations of the

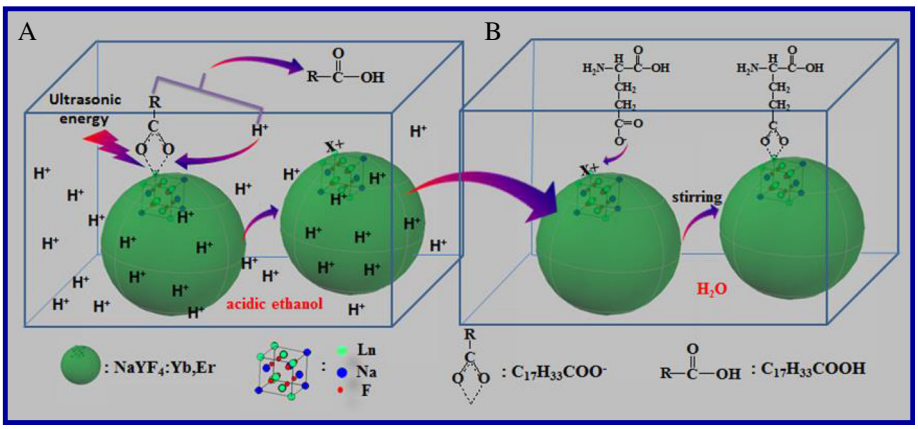

Fig. 1 The schematic diagram of oleate ligand removed from the surface of $NaYF_4$:Yb,Er NPs in the acidic ethanol (**a**) and the water-soluble new-UCNPs coupled with amino acid (**b**) in aqueous solution

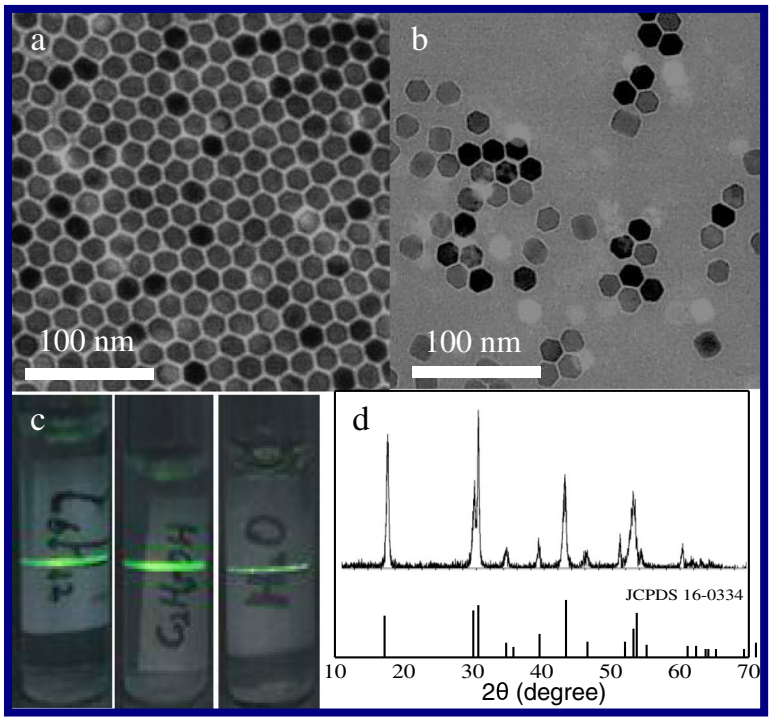

Fig. 2 a–d The TEM images, the digital pictures, and XRD spectra of as-prepared OA-capped $NaYF_4$:Yb,Er NPs and OA-free $NaYF_4$:Yb,Er NPs, respectively

methylene (CH_2) group are located at 3008 and 2923 and 2853 cm^{-1}, respectively. The C=O stretching vibration mode and the O–H stretching vibration mode of the carboxyl group are located at 1708 and 934 cm^{-1}, respectively. The curve b is the FTIR spectrum of OA-capped $NaYF_4$:Yb,Er NPs, the specific absorbing peak of the alkene stretchings (C=C), and the asymmetric and symmetric stretching vibrations of the methylene (CH_2) group located at 2923 and 2853 cm^{-1} separately with remarkable clarity in the spectrum. The absorption peaks of 1562 and 1419 cm^{-1} associate with the asymmetric and symmetric stretching vibrations of the carboxylic group ($-COO^-$), respectively, instead of the peak at 1708 cm^{-1}, which attributes to the electrostatic attraction and chemical adsorption between the Ln^{3+} ions of the surface of OA-capped $NaYF_4$:Yb,Er NPs and $-COO^-$ groups of the oleic acid. The results are lined with the previous reports [16, 55]. In Fig. 3c, the featured absorption peak of carboxyl at 1555

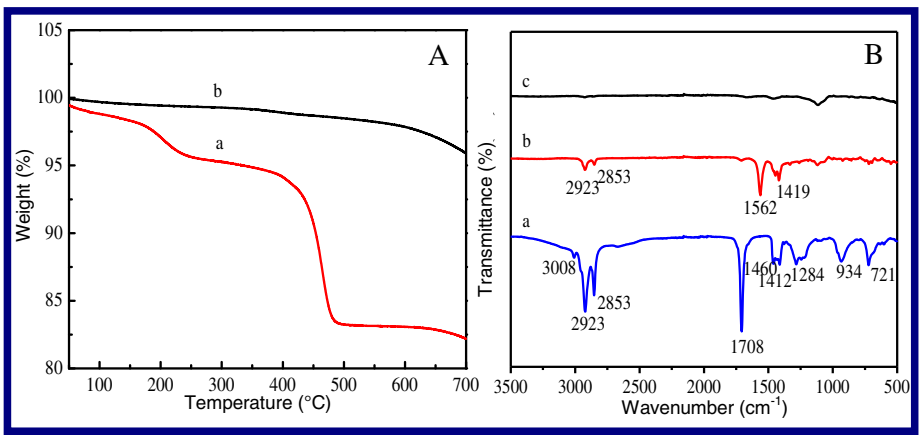

Fig. 3 a The TGA curves of $NaYF_4$:Yb,Er NPs. *a* OA-capped samples, *b* OA-free samples. **b** FTIR absorption spectra of as-prepared $NaYF_4$:Yb, Er NPs before and after removing OA layer. *a* OA, *b* OA-capped samples, *c* OA-free samples

and 1459 cm^{-1} band cannot be found, which confirms that the sample c is OA-free $NaYF_4$:Yb,Er NPs.

Figure 4 shows the ^{1}HNMR spectra of oil-soluble and water-soluble $NaYF_4$:Yb,Er NPs, respectively. Figure 4a–c is the ^{1}HNMR curves of OA dispersed in $CDCl_3$, OA-capped $NaYF_4$:Yb,Er NPs dispersed in DMSO, and OA-free $NaYF_4$:Yb,Er NPs dispersed in D_2O, respectively. As can be seen, all of the characteristic peaks of OA are one-to-one correspondence between sample A and sample B, which illustrates that the $NaYF_4$:Yb,Er NPs are coated by OA. In Fig. 4c, the peak at 4.69 ppm which attributes to H_2O from D_2O ^{1}HNMR spectra confirms that OA is removed from the surface of the NPs.

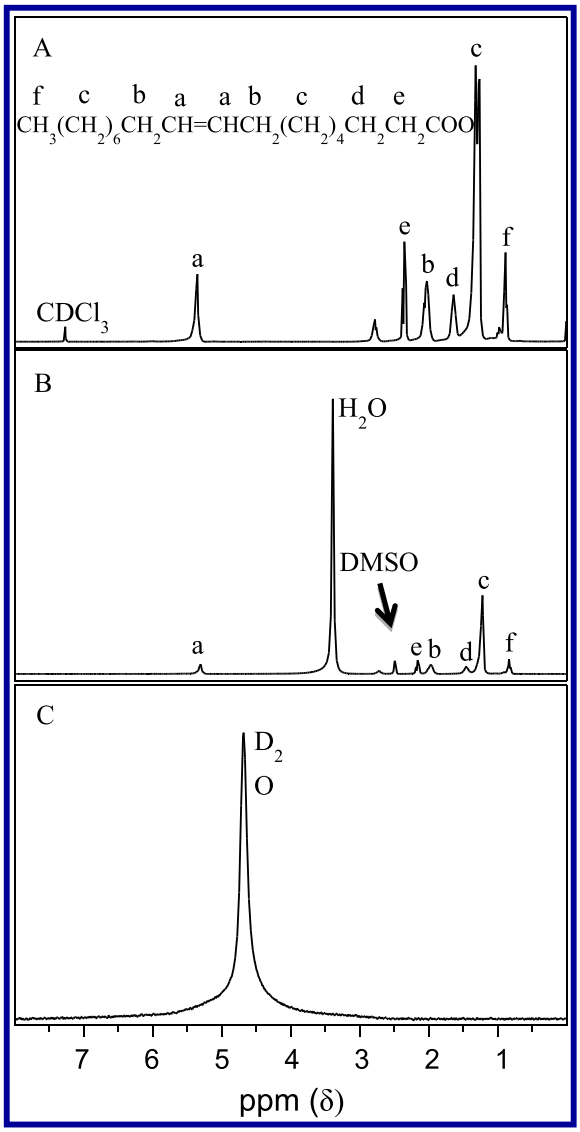

Fig. 4 ^{1}HNMR spectra of three samples. **a** OA dispersed in CDCl3. **b** OA-capped samples dispersed in DMSO. **c** OA-free samples dispersed in D_2O

The value of zeta potential (ζ) is an important parameter, which indicates the stability condition of a colloidal system and how about the dispersed state of the NPs for testing in the solution. Lü et al. reports that the colloidal system with a zeta potential of ±25 mV will become stable where there is absence of coagulation [56]. Figure 5a shows the curve of the zeta potentials of OA-free $NaYF_4$:Yb,Er NPs at different pH values. The solution of 0.1 mol/l PBS (pH = 7.4) acts as solvent to disperse the samples, which is prepared by using 0.1 mol/l Na_2HPO_4 and KH_2PO_4, HCl (0.1 mol/l) and NaOH (0.1 mol/l) which are used to adjust the pH value of the solution. As can be seen, the value of zeta potentials of the solution decreases gradually from +27.38 to −35.14 mV with the increase of pH value. At the point of zero charge, the pH value is 4.75, which corresponds to the PI isoelectric point. The value of zeta potentials of the OA-free $NaYF_4$:Yb,Er NP solution is about −27 mV when pH equals to 7.4 (physiological solution). As a result, the testing OA-free $NaYF_4$:Yb,Er NPs can disperse into aqueous solution steadily. In other words, we carry out the transformation from oil-soluble NPs to water-soluble NPs successfully.

As analysis in the mechanism section, the surface of the freshly synthesized $NaYF_4$:Yb,Er NPs exists unsaturated bonding of rear earth ions, which coordinates with the carboxy group of oleate anions to form OA-capped $NaYF_4$:Yb,Er NPs. So, the freshly prepared OA-free $NaYF_4$:Yb,Er NPs turn into positively charged particles after removing the covered layer, which can be predicted that the high activity dangling bond existed on the surface of particles will be neutralized by their storage environment if they are placed in the air for a long time and finally result in the loss of positive charge from the surface of the particles. As known, positive or negative of zeta potential represents the nanoparticles with what kind of charge according to the definition of zeta potential, normally, $\zeta > 0$ means the positively charged particles, whereas the particles carry a negative charge. Herein, we prepare two samples, one is the freshly prepared OA-free $NaYF_4$:Yb,Er NPs (new-UCNPs) and the other is OA-free $NaYF_4$:Yb,Er NPs which are placed in the air for 2 months (aged-UCNPs). The measured zeta potential of new-UCNPs is +32.96 mV under aqueous solution of pH = 6, which indicates that the new-UCNPs are positively charged particles. Though the aged-UCNPs also have excellent water-solubility, they are negatively charged particles because its measured zeta potential is −29.50 mV. The results are lined with our prediction. In consideration of the positively charged new-UCNPs possess electrophilicity, it is possible that the freshly prepared OA-free $NaYF_4$:Yb,Er NPs can react directly with negatively charged centers on biomolecules and form UCNP-biomolecule adducts.

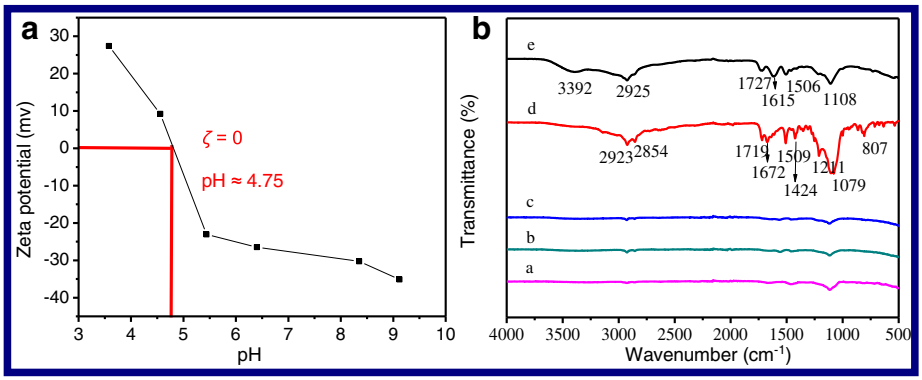

Fig. 5 **a** The curve of the zeta potentials of OA-free NaYF4:Yb,Er NPs at different pH values. **b** The FTIR spectra of the complexes of amine acid coupling with NaYF4:Yb,Er NPs. *a* new-NaYF4:Yb,Er, *b–e* new-NaYF4:Yb,Er coupled with glycine, threonine, glutamic acid, and lysine, respectively

UCNPs Couple with Amino Acid

Amino and carboxy are electron-donating group, which can attract with positively charged ions, such as the unsaturated bonding of rear earth ions exist on the surface of the new-UCNPs to form adducts. Herein, alpha-amino-beta-hydroxybutyric acid [$CH_3CH(OH)CH(NH_2)COOH$], glycine [NH_2CH_2COOH], glutamic acid [$HOOCCHNH_2(CH_2)_2COOH$], and L-lysine [$H_2NCH_2CH_2CH_2CH_2CH(NH_2)COOH$] are employed to couple with the aging-UCNPs (18 nm) and new-UCNPs (18 nm), respectively. The FTIR spectra of the complexes of amine acid coupling with $NaYF_4$:Yb,Er NPs are shown in Fig. 5b, respectively. As can be seen, curve a is the FTIR spectrum of new-UCNPs. Curves b and c (corresponding to the products of new-UCNPs react with glycine and threonine, respectively) have the same profile with curve a and absence all of the characteristic peaks of amino acid, which indicates that new-UCNPs cannot couple with glycine and threonine. For the curves d and e, the typical absorption peaks located at 2923, 2854, and 2925 cm^{-1} come from the asymmetric and symmetric stretching vibrations of the C–H bond ($-CH_2$), respectively [57]. The peaks of 1719 and 1727 cm^{-1} correspond to the typical amide carbonyl absorption band. The absorption bands located at 1615 and 1672 cm^{-1} are attributed to the N–H bending mode of amino group ($-NH_2$) [58]. The peak at 3392 cm^{-1} is attributed to the stretching vibration of amine groups. The peaks of 1424, 1506, and 1509 cm^{-1} belong to the stretching vibrations of the C–N bond. The absorption bands of 1211 cm^{-1} and (1079, 1108 cm^{-1}) belong to the C–N and C–O bond, respectively. The peaks at 807 cm^{-1} are attributed to the C–O–Y vibration [56]. All of the signals illustrate that the freshly prepared water-soluble $NaYF_4$:Yb,Er NPs have coupled with glutamic acid and lysine successfully. Why glutamic acid and lysine? Figure 6 shows the solubility equilibrium equations of the above amino acids in the aqueous solution.

As known, adjacent amino and carboxy of amino acid can form into inner-salt in the aqueous solution. So, the group of $-NH_3^+$ will act as steric hindrance to hinder the electron-donating group, carboxylate ion, to couple with positively charged ions, and leads to $CH_3CH(OH)CH(NH_2)COOH$ and NH_2CH_2COOH seldom react with new-UCNPs finally.

For $HOOCCHNH_2(CH_2)_2COOH$ and $H_2NCH_2CH_2CH_2CH_2CH(NH_2)COOH$, such as in Fig. 6 Eq. (3) and (4), one end of the molecules forms inner-salt, the existence of $-NH_3^+$ acting as steric hindrance will hinder the coupling between carboxyl and UCNPs; the other end of the molecules keeps the strong nucleophilicity group, carboxyl (Fig. 6 formula 3) and amino (Fig. 6 formula 4). Therefore, $HOOCCHNH_2(CH_2)_2COOH$ and $H_2NCH_2CH_2CH_2CH_2CH(NH_2)COOH$ can couple with newly UCNPs directly, as shown in Fig. 1b. In Fig. 5, we also notice that curve d has a higher signal of amino acid than that of curve e, which indicates that the effect of $HOOCCHNH_2(CH_2)_2COOH$ coupling with UCNPs is better than that of $H_2NCH_2CH_2CH_2CH_2CH(NH_2)COOH$. The reason may be that carboxyl nucleophilic performance is better than that of amino.

Fluorescence Labeling and Imaging of HeLa Cells

It is common sense that the cell membrane is always negatively charged, so the cationic particles tend to binding negatively charged groups on the cell surface (e.g., sialic acid, phosphate group) [59]. As positively charged particles have the greatest efficiency in cell-membrane penetration and cellular internalization, they form the primary platform as synthetic carriers for drug and gene delivery [60–62]. As mentioned, the new-UCNPs are active particles with positive charges owing to the dangling bond of Ln^{3+} (Ln = Y, Yb, Er) on the surface of particles, which should be able to bind with the negatively charged groups on the surface membranes of HeLa cells. Figure 7a shows the structure schematic

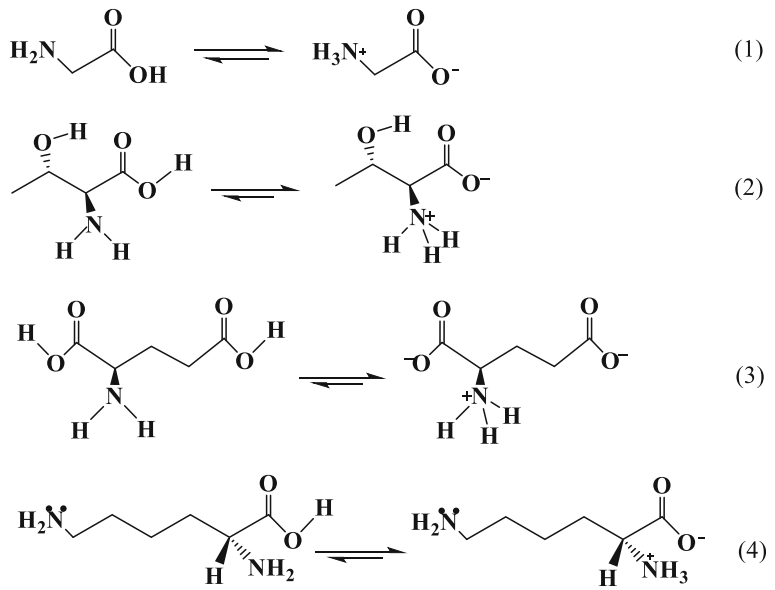

Fig. 6 The solubility equilibrium equations of alpha-amino-beta-hydroxybutyric acid, glycine, glutamic acid, and L-lysine in the aqueous solution, respectively

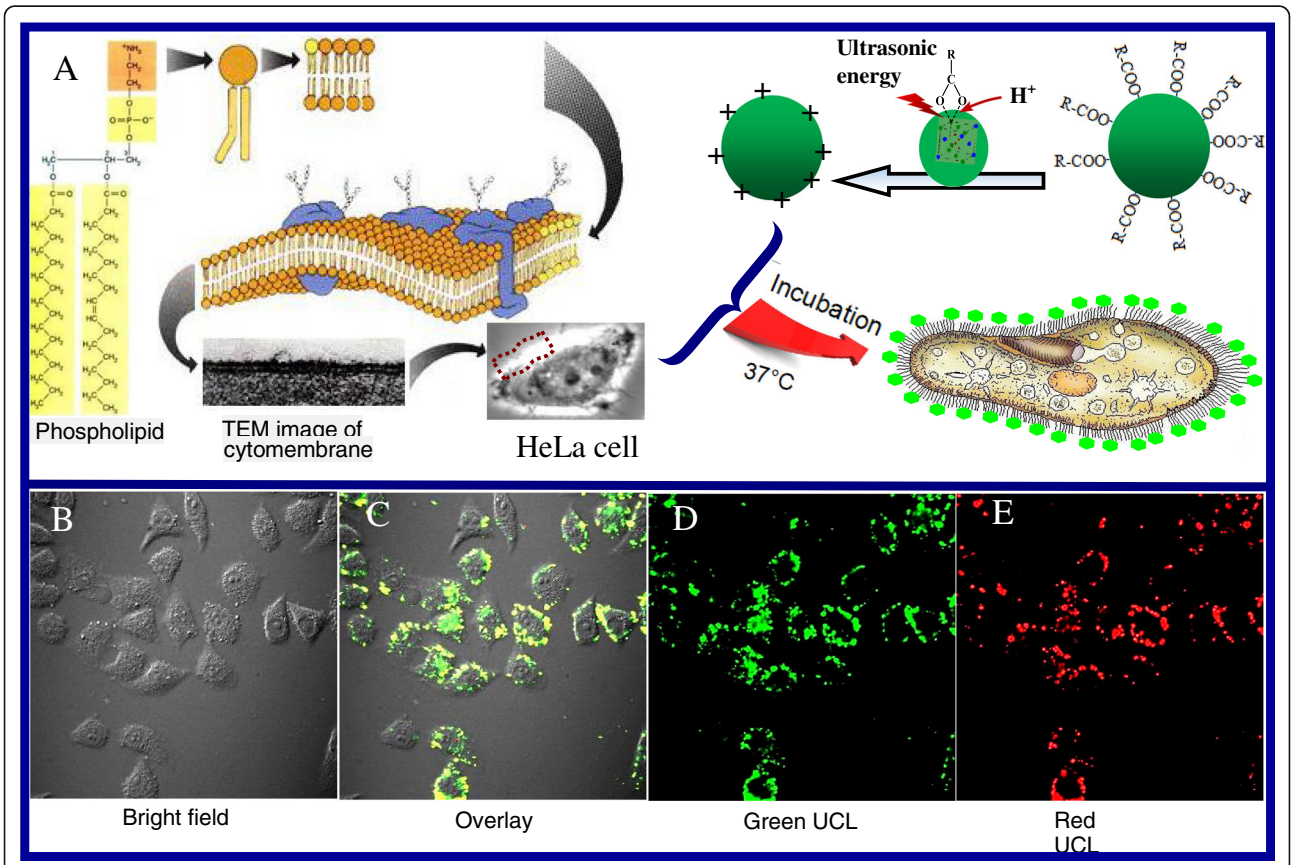

Fig. 7 a The sketch map of bio-labeling procedural of HeLa cells. **b**–**e** The confocal luminescence images of HeLa cells incubated with UCNPs at 37 °C for 16 h, respectively

diagram of HeLa cells and its bio-labeling procedure. The cytomembrane is comprised of phospholipid bilayers, as shown in Fig. 7, which have numerous negatively charged phosphate groups on the surface of phospholipid. If the new-UCNPs are incubated with HeLa live cells in physiological conditions, the coupled reaction will occur, and the new-UCNPs are thus linked to the surface of the cells. As a result, HeLa cells are labeled by $NaYF_4$:Yb,Er UCNPs.

To ascertain whether the new-UCNPs (18 nm) have been conjugated HeLa cells after incubation (C_{UCNPs} = 10 mg/ml) for 16 h at 37 °C, the cells are washed five times using PBS to get rid of the residual UCNPs thoroughly and then imaged using a confocal microscope equipped with a 980-nm NIR laser. Figure 7b–e shows the confocal luminescence images of new-UCNP-labeled HeLa cells. As is shown, the surrounding cells exhibit bright green and red UC fluorescence, confirming the attachment of the new-UCNPs conjugates on the surface of cells. The morphology and position of the cells in bright field and dark field overlap very well, showing stronger interactions between the positively charged UCNPs and the negative charged phosphate groups on the surface of phospholipid of cells. In addition, considering a long incubation time of HeLa cells with the high concentration of new-UCNPs, the labeled cells also keep considerable viability, which indicates that the new-UCNPs have good biocompatibility and low cytotoxicity. However, the biological environment is more complex, has different pH, and has the presence of proteins as well as other macrophages and nonspecific binding molecules that are everywhere in vivo model. For the consideration of our experiments just to have a specific target, the further applications in the biomedical field after addressing specificity and selectivity to target an analyte or a cell of interest should be done in the future.

Conclusions

We present an effective method to carrying out the solubility switch of nanoparticles from oil-soluble to water-soluble in terms of hydrion rivalry aided by ultrasonic; furthermore, the method is suitable for the ultra-small particles. The measured zeta potential indicates that the newly prepared OA-free $NaYF_4$:Yb,Er NPs have some positive charges, which is demonstrated to couple with amino acid and label and image the HeLa cells further. The biology experiment illustrates that the freshly prepared OA-free UCNPs can act as bio-probe for some specific target applications directly without any surface functional treatment.

Additional file

Additional file 1: Figure S1. TEM images and XRD patterns of CaF_2:Yb,Er, PbS, ZnS, and $NaGdF_4$:Yb,Er NPs of removing OA layer before and after, respectively. (DOC 1386 kb)

Acknowledgements
We are very grateful for Prof. Fuyou Li (Fudan University, China) for the help to fulfill the confocal imaging of HeLa cells. This work is supported by the National Natural Science Foundation of China (Grant No. 21445001 and 21541014), 973 Program (2013CB933800), and the Open Project of the State Key Lab of Crystal Materials, Shandong University.

Authors' Contributions
ZL is the director of the experiment group, who propounded the ideas and drafted the manuscript. HM carried out the series of experiments and characterized all the samples. YF participated in the related experiments. YL and RZ participated in the experiment of data analysis. BT participated in its design and coordination. All authors read and approved the final manuscript.

Competing Interests
The authors declare that they have no competing interests.

Received: 15 July 2016 Accepted: 21 September 2016
Published online: 01 October 2016

References

1. Mirkin CA, Letsinger RL, Mucic CR, Storhoff JJ (1996) A DNA-based method for rationally assembling nanoparticles into macroscopic materials. Nature 382:607–609
2. Seifert JL, Connor RE, Kushon SA, Wang MM, Armitage BA (1999) Spontaneous assembly of helical cyanine dye aggregates on DNA nanotemplates. J Am Chem Soc 121:2987–2995
3. Zhang F, Shi QH, Zhang YC, Shi YF, Ding KL, Zhao DY, Stucky GD (2011) Fluorescence upconversion microbarcodes for multiplexed biological detection: nucleic acid encoding. Adv Mater 23:3775–3779
4. Jin JF, Gu YJ, Man CW, Cheng JP, Xu ZH, Wang HS, Lee VH, Cheng SH, Wong W (2011) Polymer-coated $NaYF_4$: Yb^{3+}, Er^{3+} upconversion nanoparticles for charge-dependent cellular imaging. ACS Nano 5:7838–7847
5. Wang M, Mi CC, Wang WX, Liu CH, Wu YF, Xu ZR, Mao CB, Xu SK (2009) Immunolabeling and NIR-excited fluorescent imaging of HeLa cells by using $NaYF_4$:Yb,Er upconversion nanoparticles. ACS Nano 3:1580–1586
6. Park YI, Kim HM, Kim JH, Moon KC, Yoo B, Lee KT, Lee N, Choi Y, Park W, Ling D, Na K, Moon WK, Choi SH, Park HS, Yoon SY, Suh YD, Lee SH, Hyeon T (2012) Theranostic probe based on lanthanide-doped nanoparticles for simultaneous in vivo dual-modal imaging and photodynamic therapy. Adv Mater 24:5755–5761
7. Li ZS, Xu W, Wang YT, Shah BR, Zhang CL, Chen YJ, Li Y, Li B (2015) Quantum dots loaded nanogels for low cytotoxicity, pH-sensitive fluorescence, cell imaging and drug delivery. Carbohydr Polym 121:477–485
8. Wang XF, Yu WW, Zhang JY, Aldana J, Peng XG, Xiao M (2003) Photoluminescence upconversion in colloidal CdTe quantum dots. Phys Rev B 68:125318
9. Wang YF, Sun LD, Xiao JW, Feng W, Zhou JC, Shen J, Yan CH (2012) Rare-earth nanoparticles with enhanced upconversion emission and suppressed rare-earth-ion leakage. Chem Eur J 18:5558–5564
10. Yu MX, Li FY, Chen ZG, Hu H, Zhan C, Huang CH (2009) Laser scanning up-conversion luminescence microscopy for imaging cells labeled with rare-earth nanophosphors. Anal Chem 81:930
11. Hawrysz DJ, Sevick-Muraca EM (2000) Developments toward diagnostic breast cancer imaging using near-infrared optical measurements and fluorescent contrast agents. Neoplasia 2:388
12. Ntziachristos V, Bremer C, Weissleder R (2003) Fluorescence imaging with near-infrared light: new technological advances that enable in vivo molecular imaging. Eur Radiol 13:195
13. Li W, Wang JS, Ren JS, Qu XG (2013) 3D graphene oxide-polymer hydrogel: near-infrared light-triggered active scaffold for reversible cell capture and on-demand release. Adv Mater 25:6737
14. Wang YH, Wu ZG, Liu ZH (2013) Upconversion fluorescence resonance energy transfer biosensor with aromatic polymer nanospheres as the lable-free energy acceptor. Anal Chem 85:258–264
15. Kobayashi H, Ogawa M, Alford R, Choyke PL, Urano Y (2010) New strategies for fluorescent probe design in medical diagnostic imaging. Chem Rev 110:2620
16. Bogdan N, Vetrone F, Ozin GA, Capobianco JA (2011) Synthesis of ligand-free colloidally stable water dispersible brightly luminescent lanthanide-doped upconverting nanoparticles. Nano Lett 11:835–840

17. Zhang WJ, Peng B, Tian F, Qin WJ, Qian XH (2014) Facile preparation of well-defined hydrophilic core-shell upconversion nanoparticles for selective cell membrane glycan labeling and cancer cell imaging. Anal Chem 86:482–489
18. Capodilupo AL, Vergaro V, Baldassarre F, Cardone A, Corrente GA, Carlucci C, Leporatti S, Papadia P, Gigli G, Ciccarella G (2015) Thiophene-based fluorescent probes with low cytotoxicity and high photostability for lysosomes in living cells. Biochim Biophys Acta Gen Subj 1850:385–392
19. Chen GY, Ohulchanskyy TY, Liu S, Law WC, Wu F, Swihart MT, Agren H, Prasad PN (2012) Core/shell $NaGdF_4$: Nd^{3+}/$NaGdF_4$ nanocrystals with efficient near-infrared to near-infrared downconversion photoluminescence for bioimaging applications. ACS Nano 6:2969–2977
20. Liu XW, Deng RR, Zhang YH, Wang Y, Chang HJ, Huang L, Liu XG (2015) Probing the nature of upconversion nanocrystals: instrumentation matters. Chem Soc Rev 44:1479
21. Maurer-Jones MA, Gunsolus IL, Murphy CJ, Haynes CL (2013) Toxicity of engineered nanoparticles in the environment. Anal Chem 85:3036–3049
22. Shan S, Wang X, Jia N (2011) Synthesis of $NaYF_4$: Yb^{3+}, Er^{3+} upconversion nanoparticles in normal microemulsions. Nanoscale Res Lett 6:539–543
23. Heer S, Kömpe K, Güdel HU, Haase M (2004) Highly efficient multicolour upconversion emission in transparent colloids of lanthanide-doped $NaYF_4$ nanocrystals. Adv Mater 16:2102–2105
24. Yea XC, Collinsb JE, Kanga YJ, Chenc J, Chend DTN, Yodhd AG, Murray CB (2010) Morphologically controlled synthesis of colloidal upconversion nanophosphors and their shape-directed self-assembly. Proc Natl Acad Sci U S A 107:22430–22435
25. Zhou J, Liu Z, Li FY (2012) Upconversion nanophosphors for small-animal imaging. Chem Soc Rev 41:1323–1349
26. Wang X, Zhuang J, Peng Q, Li YD (2005) A general strategy for nanocrystal synthesis. Nature 437:121–124
27. Wang M, Liu JL, Zhang YX, Hou W, Wu XL, Xu SK (2009) Two-phase solvothermal synthesis of rare-earth doped $NaYF_4$ upconversion fluorescent nanocrystals. Mater Lett 63:325–327
28. Yang KS, Li Y, Yu CY, Lu LP, Ye CH, Zhang XY (2006) Upconversion luminescence properties of Ho^{3+}, Tm^{3+}, Yb^{3+} Co-doped nanocrystal $NaYF_4$ synthesized by hydrothermal method. J Rare Earths 24:757–760
29. Thorben R, Athira NR, Simon D, Markus H (2016) Synthesis of 10 nm β-$NaYF_4$: Yb, Er/$NaYF_4$ core/shell upconversion nanocrystals with 5 nm particle cores. Angew Chem Int Edit 55:1164–1167
30. Zhang F, Wan Y, Yu T, Zhang FQ, Shi YF, Xie SH, Li YG, Xu L, Tu B, Zhao DY (2007) Uniform nanostructured arrays of sodium rare-earth fluorides for highly efficient multicolor upconversion luminescence. Angew Chem Int Edit 46:7976–7979
31. Mai HX, Zhang YW, Si R, Yan ZG, Sun LD, You LP, Yan CH (2006) High-quality sodium rare-earth fluoride nanocrystals: controlled synthesis and optical properties. J Am Chem Soc 128:6426–6436
32. Wang LY, Li YD (2007) Controlled synthesis and luminescence of lanthanide doped $NaYF_4$ nanocrystals. Chem Mater 19:727–734
33. Wang LY, Li YD (2006) $Na(Y_{1.5}Na_{0.5})F_6$ single-crystal nanorods as multicolor luminescent materials. Nano Lett 6:1645–1649
34. Michalet X, Pinaud FF, Bentolila LA, Tsay JM, Doose S, Li JJ, Sundaresan G, Wu AM, Gambhir SS, Weiss S (2005) Quantum dots for live cells, in vivo imaging, and diagnostics. Science 307:538–544
35. Gao XH, Cui YY, Levenson RM, Chung LWK, Nie S (2004) In vivo cancer targeting and imaging with semiconductor quantum dots. Nat Biotechnol 22:969–976
36. Chen EY, Daley D, Wang Y, Garnica M, Chen CS, Chin WC (2012) Functionalized carboxyl nanoparticles enhance mucus dispersion and hydration. Sci Rep 2:211–215
37. Han MY, Gao XH, Su JZ, Nie SM (2001) Quantum-dot-tagged microbeads for multiplexed optical coding of biomolecules. Nat Biotechnol 19:631–635
38. Liu SJ, Zhang LL, Yang TS, Yang HR, Zhang KY, Zhao X, Lv W, Yu Q, Zhang XL, Zhao Q, Liu XM, Huang W (2014) Development of upconversion luminescent probe for ratiometric sensing and bioimaging of hydrogen sulfide. ACS Appl Mater Interfaces 6:11013–11017
39. Tu NN, Wang LY (2013) Surface plasmon resonance enhanced upconversion luminescence in aqueous media for TNT selective detection. Chem Commun 49:6319–6321
40. Dong A, Ye X, Chen J, Kang Y, Gordon T, Kikkawa JM, Murray CB (2011) A generalized ligand-exchange strategy enabling sequential surface functionalization of colloidal nanocrystals. J Am Chem Soc 133:998–1006
41. Medintz IL, Stewart MH, Trammell SA, Susumu K, Delehanty JB, Mei BC, Melinger JS, Blanco-Canosa JB, Dawson PE, Mattoussi H (2010) Quantum-dot/dopamine bioconjugates function as redox coupled assemblies for in vitro and intracellular pH sensing. Nat Mater 9:676–684
42. Ma Y, Chen ML, Li MY (2015) Hydrothermal synthesis of hydrophilic $NaYF_4$: Yb, Er nanoparticles with bright upconversion luminescence as biological label. Mater Lett 139:22–25
43. Pichaandi J, Boyer JC, Delaney KR, van Veggel FCJM (2011) Two-photon upconversion laser (scanning and wide-field) microscopy using Ln^{3+}-doped $NaYF_4$ upconverting nanocrystals: a critical evaluation of their performance and potential in bioimaging. J Phys Chem C 115:19054–19064
44. Shariat M, Raftari M, Bakar FA (2013) Evaluation of sensory and biochemical changes in freshwater catfish stored under vacuum and different modified atmospheres. Anal Methods 5:231–238
45. Liu Y, Chen M, Cao TY, Sun Y, Li CY, Liu Q, Yang TS, Yao LM, Feng W, Li FY (2013) A cyanine-modified nanosystem for in vivo upconversion luminescence bioimaging of methylmercury. J Am Chem Soc 135:9869–9876
46. Chen J, Guo CG, Wang M, Huang L, Wang LP, Mi CC, Li J, Fang XX, Mao CB, Xu SK (2011) Controllable synthesis of $NaYF_4$: Yb, Er upconversion nanophosphors and their application to in vivo imaging of Caenorhabditis elegans. J Mater Chem 21:2632–2638
47. Liu JL, Cheng JT, Zhang Y (2013) Upconversion nanoparticle based LRET system for sensitive detection of MRSA DNA sequence. Biosens Bioelection 43:252–256
48. Zhou HP, Xu CH, Sun W, Yan CH (2009) Clean and flexible modification strategy for carboxyl/aldehyde-functionalized upconversion nanoparticles and their optical applications. Adv Funct Mater 24:3892–3900
49. Hu H, Yu MX, Li FY, Chen ZG, Gao X, Xiong LQ, Huang CH (2008) Facile epoxidation strategy for producing amphiphilic up-converting rare-earth nanophosphors as biological labels. Chem Mater 20:7003–7009
50. Chen ZG, Chen HL, Hu H, Yu MX, Li FY, Zhang Q, Zhou ZG, Yi T, Huang CH (2008) Versatile synthesis strategy for carboxylic acid-functionalized upconverting nanophosphors as biological labels. J Am Chem Soc 130:3023–3029
51. Wang LY, Yan RX, Huo ZY, Wang L, Zeng JH, Bao J, Wang X, Peng Q, Li YD (2005) Fluorescence resonant energy transfer biosensor based on upconversion-luminescent nanoparticles. Angew Chem Int Edit 44:6054–6057
52. Li ZH, Li Y, Wang YN, Miao HX, Du Y, Liu H (2014) A general strategy to fabricate ligand-free water-soluble up-conversion nanoparticles. J Alloys Compd 613:18–24
53. Ohlson M, Sorensson J, Haraldsson B (2000) Glomerular size and charge selectivity in the rat as revealed by FITC-Ficoll and albumin. Am J Physiol Renal Physiol 279:84–91
54. Longmire M, Choyke PL, Kobayashi H (2008) Clearance properties of nano-sized particles and molecules as imaging agents: considerations and caveats. Nanomedicine 3:703–717
55. Costa D, Burrows HD, Miguel MDG (2005) Changes in hydration of lanthanide ions on binding to DNA in aqueous solution. Langmuir 21: 10492–10496
56. Lü Q, Li AH, Guo FY, Sun L, Zhao LC (2008) Experimental study on the surface modification of Y_2O_3: Tm^{3+}/Yb^{3+} nanoparticles to enhance upconversion fluorescence and weaken aggregation. Nanotechnology 19: 145701–145709
57. Yi ZG, Zeng SJ, Lu W, Wang HB, Rao L, Liu HR, Hao JH (2014) Synergistic dual-modality in vivo upconversion luminescence/X-ray imaging and tracking of amine-functionalized $NaYbF_4$:Er nanoprobes. ACS Appl Mater Interfaces 6:3839–3846
58. Ju Q, Tu DT, Liu YS, Li RF, Zhu HM, Chen JC, Chen Z, Huang MD, Chen XY (2012) Amine-functionalized lanthanide-doped $KGdF_4$ nanocrystals as potential optical/magnetic multimodal bioprobes. J Am Chem Soc 134: 1323–1330
59. Cho EC, Xie JW, Wurm PA, Xia YN (2009) Understanding the role of surface charges in cellular adsorption versus internalization by selectively removing gold nanoparticles on the cell surface with a I_2/KI etchant. Nano Lett 9:1080–1084
60. Martin AL, Bernas LM, Rutt BK, Foster PJ, Gillies ER (2008) Enhanced cell uptake of superparamagnetic iron oxide nanoparticles functionalized with dendritic guanidines. Bioconjugate Chem 19:2375–2384
61. Harush-Frenkel O, Debotton N, Benita S, Altschuler Y (2007) Targeting of nanoparticles to the clathrin-mediated endocytic pathway. Biochem Biophys Res Commun 353:26–32
62. Lee J, Kim J, Park E, Jo S, Song R (2008) PEG-ylated cationic CdSe/ZnS QDs as an efficient intracellular labeling agent. Phys Chem Chem Phys 10:1739–1942